Structure-Based Optimization of Nonquaternary Reactivators of Acetylcholinesterase Inhibited by Organophosphorus Nerve Agents

Gianluca Santoni, J. de Sousa, Eugenio de La Mora, J. Dias, Ludovic Jean, J.L. Sussman, I. Silman, Pierre-Yves Renard, R.C.D. Brown, Martin Weik, et al.

Structure-based optimization of non-quaternary reactivators of acetylcholinesterase inhibited by organophosphorus nerve agents

Gianluca Santoni[a,b,§], Julien de Sousa[c,d,§], Eugenio de la Mora[a,§], José Dias[b], Ludovic Jean[e], Joel L. Sussman[f], Israel Silman[g], Pierre-Yves Renard[e], Richard C. D. Brown[d], Martin Weik[a], Rachid Baati[c] and Florian Nachon[b,*]

[a] Univ. Grenoble Alpes, CEA, CNRS, IBS, F-38000 Grenoble

[b] Département de Toxicologie et Risques Chimiques, Institut de Recherche Biomédicale des Armées, 91220 Brétigny-sur-Orge, France

[c] Université de Strasbourg, ICPEES, UMR CNRS 7515, 67087 Strasbourg, France

d University of Southampton, Department of Chemistry, Highfield, Southampton, SO17 1BJ, United Kingdom

[e] Université de Normandie, COBRA, UMR 6014, FR 3038, Université de Rouen, INSA de Rouen, CNRS, 76821 Mont-Saint-Aignan, France.

[f] Department of Structural Biology, Weizmann Institute of Science, 76100 Rehovot, Israel.

[g] Department of Neurobiology, Weizmann Institute of Science, 76100 Rehovot, Israel.

Abstract

Acetylcholinesterase (AChE), a key enzyme in the central and peripheral nervous systems, is the principal target of organophosphorus nerve agents. Quaternary oximes can regenerate AChE activity by displacing the phosphyl group of the nerve agent from the active-site, but they poorly distribute in the central nervous system. A promising reactivator based on tetrahydroacridine linked to a non-quaternary oxime is also an undesired sub-micromolar reversible inhibitor of AChE. X-ray structures and molecular docking indicate that structural modification of tetrahydroacridine might decrease inhibition without affecting reactivation. The chlorinated derivative was synthesized, and, in line with the prediction, displayed a 10-fold decrease in inhibition, but no significant decrease in reactivation efficiency. X-ray structures with the derivative rationalize this outcome. We thus show that rational design based on structural studies permits the refinement of a new generation pyridine aldoxime reactivators that may be more effective in the treatment of nerve agent intoxication.

Introduction

Acetylcholinesterase (AChE) is found at cholinergic synapses throughout the nervous system, and at the neuromuscular junction. Its principal role is to terminate the synaptic transmission by rapid hydrolysis of the neurotransmitter acetylcholine (ACh) [1]. AChE is the principal target of organophosphate (OP) pesticides and nerve agents. Although use of nerve agents has been restricted by international conventions, they remain a serious threat, as demonstrated by the sarin attack at Khan Sheikhoun in Syria in april 2017, the assassination of Kim Jong-nam in february 2017 in Malaysia with VX and the poisoning of Serguei Skripal in march 2018 in England with a Novichok. The standard treatment for nerve agent intoxication consists of an antimuscarinic (atropine), an anticonvulsivant (usually diazepam), and a pyridinium oxime reactivator of the phosphylated AChE. Pyridinium oximes are sufficiently nucleophilic to displace the phosphyl group from AChE's active-site serine [2], but despite 60 years of research [2, 3] they display major drawbacks in terms of bioavailability in the central nervous system [4] and a restricted spectrum of action and effectiveness [5]. In particular, the permanent charge on the pyridinium severely limits passage through the blood–brain barrier (BBB) [6]. For the bioavailability of 2-pyridinealdoxime (2–PAM) has been estimated to be only 10% of that in the bloodstream in rat brain as measured by *in vivo* microdialysis coupled with HPLC/UV [4]. Furthermore, most reactivators are ineffective against tabun poisoning, none of them has proved to be equally effective against all other types of OP-AChE conjugates, and they are incapable of reactivating "aged" OP-AChE conjugates [5].

Toxogonin was one the first bifunctional oximes to be synthesized and investigated [7]. Numerous elongated ligands, containing either one or two oxime moieties at their extremities, including the Hagendorn oximes, have since been studied as AChE reactivators [8-10]. Now that the crystal structures of *Tc*AChE [11] and mammalian AChEs [12] have become available, it is realized that such elongated oximes span the active-site gorge, bridging between the catalytic

aromatic site (CAS) and the peripheral aromatic site (PAS). However, structural studies, such as those of Ekström and colleagues [13, 14], have shown that binding of oximes within the active-site gorge of AChE is far from optimal for reactivation.

In an earlier study [15], we reported the design, synthesis and reactivation properties of a new class of bifunctional reactivators in which the moiety interacting with the PAS is based on tetrahydroacridine (Figure 1). The lead reactivator molecule, **1,** reversibly inhibits AChEs in the submicromolar range. Though it is not yet clear whether this could prejudice its *in vivo* efficacy as a reactivator, we wished to explore ways of decreasing inhibitor potency without concomitant loss of reactivator efficacy. First, based on crystallographic structures of complexes of **1** with apo, nerve agent-inhibited, and carbamylated *Tc*AChE we identified the structural basis for its high inhibitory potency. This permitted us to design an improved molecule, reactivator **2,** that successfully prevents the binding mode responsible for the submicromolar inhibition of the apo enzyme, without altering the reactivating capacity. Kinetic measurements, together with structural studies, confirmed the success of our strategy.

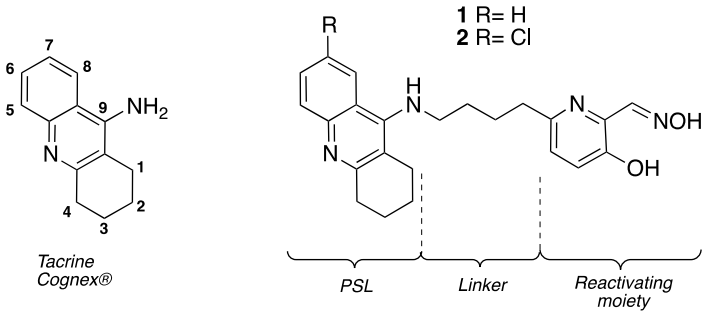

Figure 1 Chemical structures of tacrine and uncharged hybrid reactivators **1** and **2**.

Results and discussion

Chemistry

Following the route established by Baati and co-workers [15], the synthesis of the reactivator, **2,** is herein described. Our initial efforts focused on the synthesis of the PSL scaffold. *N*-Alkylation of 9-aminotacrine proved not to be a reliable method [16, 17]. A new strategy was devised that involved use of a novel electrophilic compound, 7-chloro-1,2,3,4-tetrathydroacridin-9-yl trifluoromethanesulfonate, **5** (Scheme 1) [18]. Starting from commercially available 5-chloroanthranilic acid, 7,9-dichloro-1,2,3,4-tetrahydroacridine, **3**, was obtained by Lewis Acid-mediated intermolecular cyclodehydration with cyclohexanone. This intermediate, **4**, was subsequently hydrolyzed using glacial acetic acid at 200 °C in a sealed tube. This two-step synthetic sequence proved to be superior to the more frequently reported direct condensation reactions of anthranilic acids and cycloalkanone via azeotropic distillation of water [19]. Then, triflation allowed isolation of the desired 7-chloro-1,2,3,4-tetrathydroacridin-9-yl trifluoromethanesulfonate, **5,** in an excellent overall yield (Scheme 1).

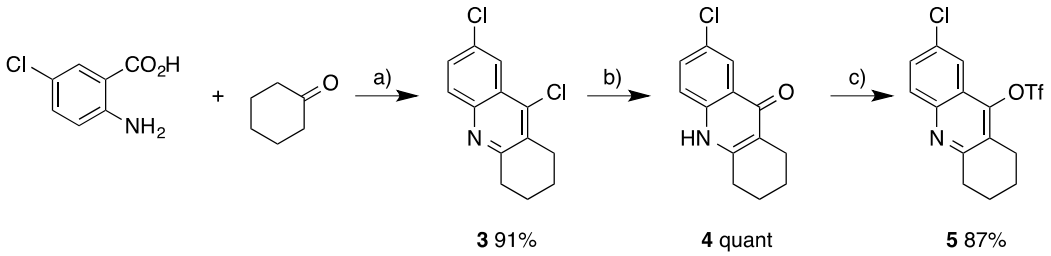

Scheme 1 Synthesis of the trifluoromethanesulfonate 5. Conditions and reagents: (a) $POCl_3$, cyclohexanone, Δ, 16 h; (b) AcOH, 200 °C, 24 h; (c) Tf_2O, Et_3N, CH_2Cl_2, –78 °C for 1 h then RT for 16 h**.**

Introduction of the linker was achieved using our optimized microwave assisted Pd-catalysed Buchwald-Hartwig amination procedure [18] to afford the desired terminal alkynes in excellent yields (Scheme 2). Subsequent Sonogashira coupling with methyl 3-benzyloxy-6-bromopicolinate [20] proceeded well to generate the corresponding hybrid precursors. Then, a *one-pot* alkyne reduction and *O*-debenzylation under hydrogen in the presence of Pearlman's

catalyst afforded the 3-hydroxypyridine derivatives **8**. The latter was converted into the corresponding oxime using a three-step sequence involving TBS protection of the phenolic group, reduction of the methyl ester to an aldehyde function with DIBAL-H, and subsequent oxime formation by condensation with hydroxylamine (Scheme 2). The desired hybrid was thus obtained in 10 steps in an overall 7% yield.

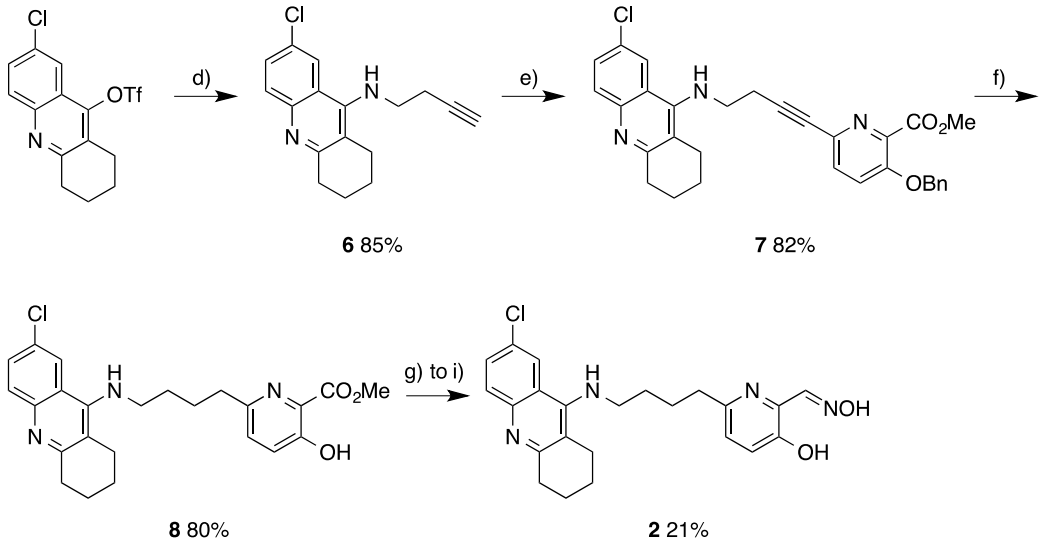

Scheme 2 Synthesis of the hybrid reactivator 2. Conditions and reagents: (d) 1-amino-3-butyne, $Pd_2(dba)_3$, (±)-BINAP, Cs_2CO_3, 1,4-dioxane, μW (100 °C, 1 h); (e) methyl 3-benzyloxy-6-bromopicolinate, $Pd[PPh_3]_4$, CuI, THF/Et_3N, rt, 16 h; (f) H_2 (1 atm), $Pd(OH)_2$/C, EtOAc, rt, 7 h; (g) TBSOTf, 2,6-lutidine, CH_2Cl_2, rt, 2 h; (h) DIBAL–H, CH_2Cl_2, –78 °C, 12 min; (i) $NH_2OH.HCl$, NaOAc, EtOH, Δ, 15 h.

It is noteworthy that during the synthesis of the hybrid, the phenolic TBS group was found to be quite labile, mainly due to electron deficiency of the pyridine system that determines the strength of the Si–O bond. This observation was turned to our advantage since, after the DIBAL–H reduction, a work-up using aqueous 1 M NaOH sufficed to deprotect the silyloxy intermediate, and thus avoid using a toxic fluoride-containing reagent.

X-ray structures of compound 1 in complex with *Tc*AChE and with OP/*Tc*AChE conjugates.

To optimize a reactivator, detailed structural information is important for designing the improved version. Both the structures of the *Tc*AChE-**1** complex and of the NEDPA-*Tc*AChE-

1 ternary complex were solved in order to provide such information. Data collection and refinement statistics for all the structures of the present article are reported in Table 1.

Table 1 Data collection and refinement statistics. Calculated using Phenix (Adams *et al* Acta Cryst. D 2010;66:213-221). R-work=Σ |Fo - |Fc|| / Σ |Fo|, Fo and Fc are observed and calculated structure factors, R-free set uses about thousands randomly chosen reflections. Statistics for the highest-resolution shell are shown in parentheses.

Complex	Tabun-*Tc*AChE	*Tc*AChE-**1**	NEDPA-*Tc*AChE-**1**	*Tc*AChE-**2**	NEDPA-*Tc*AChE-**2**	Carbamyl-*Tc*AChE-**1**	Carbamyl-*Tc*AChE-**2**
PDB code	6g17	6g4m	6g4o	6g4n	6g4p	6fld	6fqn
Data Collection							
Resolution Range (Å)	45.7-2.2 (2.28-2.20)	45.91-2.63 (2.72-2.63)	58.14-2.90 (3.00-2.90)	46.3-2.90 (3.0-2.9)	45.92-2.72 (2.82-2.72)	37.32-2.40 (2.49-2.40)	37.13-2.3 (2.38-2.3)
Space group	P3121	P212121	P212121	P212121	P212121	P3121	P3121
Unit cell parameters (Å)	111.8 111.8 137.2	91.3 106.2 150.5	91.5 106.4 150.5	91.8 107.2 150.4	91.83 107.4 151.2	114.01 114.01 136.98	113.43 113.43 137.57
Total Reflections	274775 (27951)	214755 (21464)	150232 (15096)	212283 (21557)	173389 (17585)	280500 (27774)	318401 (30477)
Unique Reflections	50213 (5024)	43964 (4317)	32837 (3215)	33562 (3300)	40508 (3947)	40569 (3956)	45946 (4513)
Multiplicity	5.5 (5.6)	4.9 (5.0)	4.6 (4.7)	6.3 (6.5)	4.3 (4.5)	6.9 (7.0)	6.9 (6.7)
Completeness %	98.8 (98.5)	99.5 (99.4)	98.7 (99.1	99.9 (99.9)	99.2 (99.9)	99.7 (97.9)	99.7 (99.7)
Mean I/sigma(I)	13.7 (2.2)	9.2 (1.9)	9.20 (2.3)	10.1 (2.9)	3.8 (0.8)	14.3 (2.2)	11.3 (2.3)
$CC_{1/2}$	0.99 (0.92)	0.99 (0.74)	0.99 (0.85)	0.99 (0.90)	0.95 (0.38)	0.99 (0.87)	0.99 (0.81)
Refinement							
Rwork (%)	17.5 (32.7)	19.0 (28.2)	18.5 (25.4)	19.4 (27.2)	21.0 (33.6)	18.3 (31.5)	20.5 (39.0)
Rfree (%)	21.6 (33.7)	26.5 (37.2)	26.1 (33.2)	26.6 (31.5)	28.0 (43.1)	21.4 (37.6)	23.4 (38.2)
RMS bond length	0.008	0.009	0.009	0.097	0.009	0.011	0.007
RMS bond angles	1.08	1.2	1.2	2.28	1.27	0.99	1.00
Total atoms	4784	9139	8856	9051	8679	4577	4540
Ramachandran							
favorable	96	94	92	92	92	95	94
outliers	0.19	0.28	0.47	0.19	1.0	0.19	0.76
Average B-factor (A^2)	42.0	35	39.5	32.5	37.2	52.2	51.4

First, we solved the structure of the non-aged form of the tabun-*Tc*AChE conjugate, which could serve as a template for subsequent refinements. Crystals of the conjugate were obtained by a 2-min soak of the native trigonal *Tc*AChE crystals in mother liquor containing 0.5 mM

tabun. Figure 2 shows the similarity of this structure to those of the tabun conjugates of mAChE and hAChE [21].

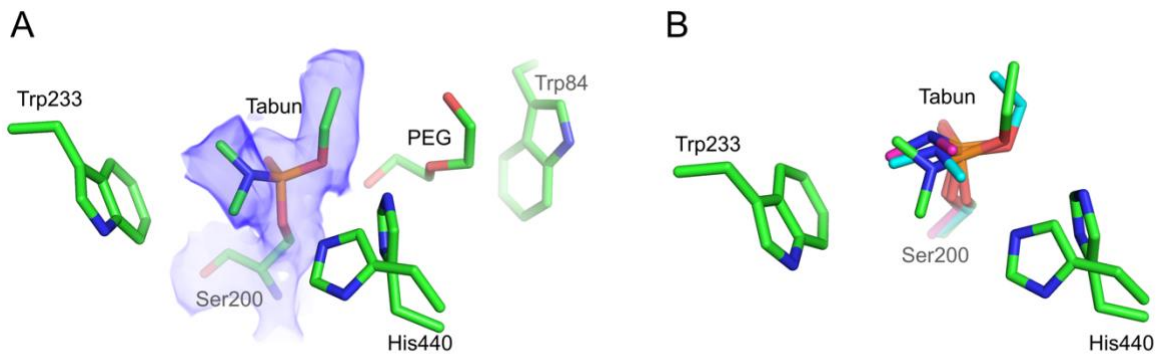

Figure 2 A) Structure of the non-aged tabun-*Tc*AChE conjugate (pdb 6g17). Volume representation of the feature enhanced map (fem) around the catalytic serine contoured at 1 σ, showing the phosphyl moiety attached to Ser200. His440 is observed in two alternate conformations with equal occupancy; B) Superimposition of the phosphylated catalytic serine of non-aged tabun-*Tc*AChE (pdb 6g17, green), tabun-mAChE (pdb 3dl4, cyan) and the aged tabun-hAChE conjugate (pdb 2x8b, magenta). The orientation of the dimethylamino group of tabun is similar in all three structures, suggesting that also in *Tc*AChE aging occurs via loss of the ethyl group.

In all three structures the dimethylamino group of tabun is located in the acyl binding pocket, and the O2 oxygen atom is stabilized within the oxyanion hole. These structural findings support the notion that the tabun-AChE conjugate ages by O-dealkylation. The ethyl group of tabun points toward Trp84, at the bottom of the gorge, thus inducing rotation of His440 to adopt a non-native conformation that had been observed previously in other non-aged OP conjugates [22, 23]. The presence of the tabun moiety combined with this alternate conformation of His440 reduces by 15% the solvent accessible volume of the active-site gorge with respect to the native enzyme. PEG molecules from the mother liquor occupy the remaining accessible volume at the bottom of the gorge and at the PAS [24].

The structure of the complex of reactivator **1** with orthorhombic *Tc*AChE is shown in Figure 3A.

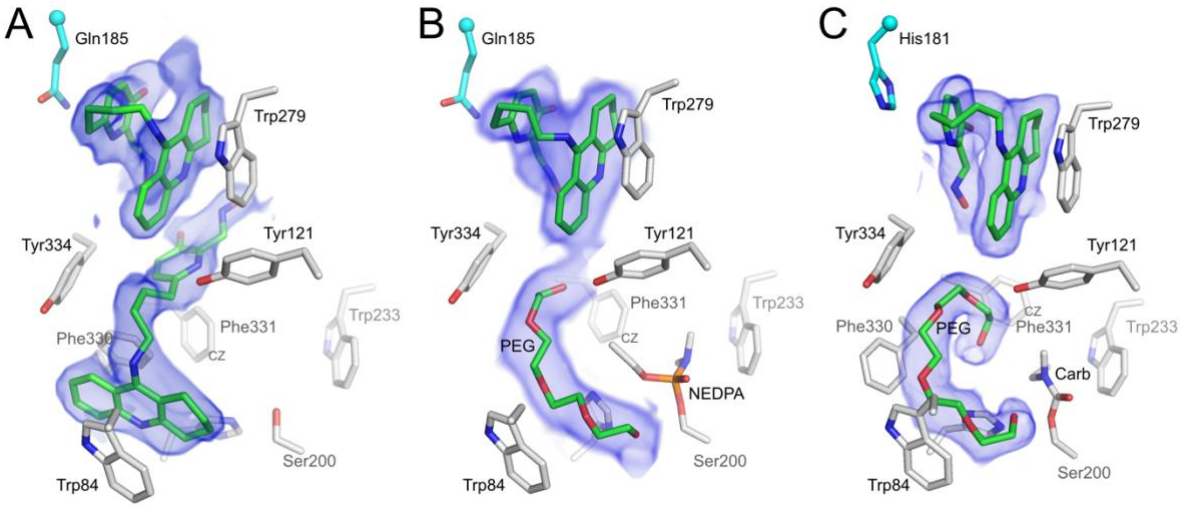

Figure 3 Crystal structures of unmodified *Tc*AChE and of its conjugates complexed with **1**. Volume represents feature enhanced maps (fem) contoured at 1 σ. A) *Tc*AChE-**1** complex obtained from orthorhombic crystals (pdb 6g4m). Two copies of 1 are seen, one at the bottom of the gorge, and one at the PAS; B) NEDPA-*Tc*AChE-**1** complex obtained from orthorhombic crystals (pdb 6g4o). A copy of **1** is seen at the PAS, and a PEG oligomer is seen alongside the phosphyl group at the bottom of the gorge; C) Carbamyl-*Tc*AChE-**1** complex, obtained from trigonal crystals (pdb 6fld). A copy of **1** is seen at the PAS, and a PEG oligomer is seen alongside the carbamyl group at the bottom of the gorge. The binding orientation of **1** at the PAS in the 3 panels is stabilized by Gln185 or His181 (cyan) of a symmetry mate specific of the crystal packing, thus partially artefactual.

In each of the two monomers in the asymmetric unit two molecules of **1** are observed within the gorge, which displace PEG oligomers that are otherwise present in the gorge of the crystalline enzyme. One of these oligomers is located at the bottom of the gorge, near the catalytic triad. The tacrine moiety of **1** is oriented just as in the tacrine-*Tc*AChE complex [25]. The linker points towards the entrance of the gorge, with the oxime moiety positioned below the PAS. It is noteworthy that the oxime function does not lie in the plane of the pyridine, as it does in the energy-optimized molecule, but appears to be at an angle of 40° to the aromatic ring. At the PAS, a second copy of **1** is positioned such that the tacrine moiety stacks against the indole of Trp279, and the linker makes a U-turn, as a consequence of which its pyridinaldoxime ring stacks against its tacrine moiety. Indeed, the linker and the pyridinaldoxime cannot extend down into the gorge due to the presence of the first copy at the

CAS. The conformation of the pyridinaldoxime in the second copy seems to be stabilized by interaction with Gln185 (cyan sticks in Figure 3A) of a symmetry-related copy of the protein. The resolution of the structure is not high enough to permit assignment of the orientation of the tacrine moiety of the second copy; thus, the aromatic and saturated rings might be inverted. This holds true for all the subsequent structures presented.

NEDPA is a *p*-nitrophenyl homolog of tabun with reduced toxicity; it is assumed, however, to produce an identical AChE conjugate [26], thus making it a useful surrogate. We solved the structure of the NEDPA-*Tc*AChE-**1** ternary complex by successively soaking native orthorombic *Tc*AChE crystals in NEDPA, and then in NEDPA plus **1,** with the objective of observing the complex of **1** with the conjugate prior to reactivation (Figure 3B). As we had assumed, NEDPA forms an adduct identical to that obtained with tabun, with its dimethylamino group located in the acyl-binding pocket. The presence of the phosphyl adduct prevents the binding of **1** at the bottom of the gorge and stabilizes a PEG molecule also interacting with Trp84. A copy of **1** is seen to be bound at the PAS of monomer B with the pyridinaldoxime group stacked against the tacrine moiety, in a non-productive state (Figure 3B), in a similar orientation to that seen at the PAS in the *Tc*AChE-**1** complex (Figure 3A). However, no copy of **1** is observed at the PAS of monomer A. Instead, a large PEG oligomer spans all the space from the active site to the PAS, occupying all the available space (not shown).

To further explore how modification of the active-site serine impacts the binding of **1**, we solved the structure of a ternary complex of **1** with carbamylated *Tc*AChE obtained with a trigonal crystal. Carbamylation was achieved using a rivastigmine analog, resulting in Ser200 being modified by an *N*,*N*-ethylmethyl carbamyl group. The ethyl group of the carbamyl moiety induces a rearrangement of the acyl-loop with the sidechain of Phe288 being rotated by 110° around χ_1 (bond CA-CB), resulting in displacement of Phe331 towards the acyl-binding pocket, with its CZ atom moving 3.6 Å. The carbamyl residue significantly reduces the

accessible volume at the bottom of the gorge compared to the apo enzyme. Thus, a PEG molecule occupies the remaining space, while a molecule of **1** occupies the PAS (Figure 3C), as in the *Tc*AChE-**1** (Figure 3B) and NEDPA-*Tc*AChE-**1** (Figure 3C) complexes. Due to the different packing of trigonal compared to orthorhombic crystals, the closest symmetry-related residue stabilizing the pyridinaldoxime's conformation is His181 rather than Gln185.

Design and docking of reactivator 2

The structural data presented above showed that the tacrine moiety of reactivator **1** can bind both at the PAS and the CAS of the free enzyme. We conjectured that binding at the CAS is responsible for the inhibitory potency of **1**. We wished to modify **1** so as to prevent its binding at the CAS while preserving its capacity to binding at the PAS, and thus its affinity for the phosphylated enzyme. Careful inspection of the structure of the *Tc*AChE-**1** complex suggests that introducing a chlorine atom at position 7 on the tacrine moiety would create a steric clash with Trp432 when the ligand was bound at the active site (Figure 4A).

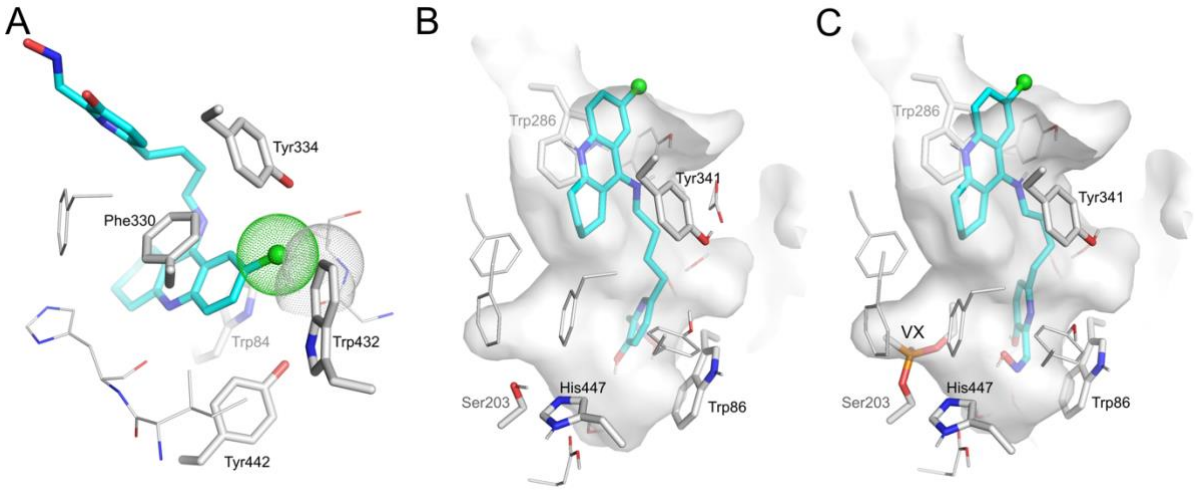

Figure 4 A) Model based on the structure of *Tc*AChE-**1** complex (pdb 6g4m) showing the steric clash between Trp432 and **1** in which the tacrine moiety has been modified by a chlorine atom at position 7 yielding **2**. The van der Waals volumes are represented as dotted spheres; B) Docking of **2** in human AChE (pdb 4ey4); C) Docking of **2** in a model of VX-inhibited hAChE (pdb 4ey4). Both docking predict that the chlorine substituent of **2** prevent binding at the bottom of the gorge but permit binding at the PAS.

This possibility was tested by molecular docking. Both **1** and the new reactivator proposed, **2**, were docked into both native and VX-inhibited hAChE. Examination of the binding modes indicates that **2** does not bind at the CAS, but only at the PAS, thus confirming the validity of the design prediction (Figure 4B-C). The estimated binding energies for the best pose suggest that **2** is a weaker inhibitor than **1 (**respectively -10.1 and -13.3 kcal/mol). Furthermore, the binding energy of **2** for VX-inhibited AChE is in the same order o fmagnitude than that of **1** indicating that binding to phosphylated AChE has been preserved (respectively -13.1 and -11.7 kcal/mol).

In vitro evaluation of reactivators 1 and 2

The reference oximes are 2–PAM, which is utilized by the French and US Military [2], obidoxime used by the German forces, and HI-6, a Hagendorn oxime, which has been investigated by the Canadian forces due to its effectiveness against soman intoxication [8]. We measured the half-maximal inhibitory concentration (IC_{50}) of the reference oximes and reactivators **1** and **2** (Table 1). Introduction of the chlorine atom reduced the affinity for the native enzyme by almost 10-fold, up to the low micromolar range. This remains 1 to 2 orders higher than the reference oximes.

Table 1 half-maximal inhibitory concentration (IC_{50}) concentration for hAChE

Reactivators	2–PAM	HI-6	Obidoxime	**1**	**2**
IC50 (µM)	560 ±30	54 ±5	640 ±70	0.25±0.02	2.3±0.2

1 and **2** were then tested for their capacity to reactivate the conjugates of hAChE with VX, tabun, paraoxon, and the NIMP surrogate of sarin. For each of these OPs, we measured the second–order rate constant for reactivation (k_{r2}), which is the ratio of the maximal reactivation rate constant (k_r) and the apparent dissociation constant of the reactivator/phosphyl–AChE complex (K_D). These measurements were made using the Ellman procedure, at pH 7.4 and 37

°C, *viz.*, close to the physiological conditions [15, 27]. The reactivation kinetics constants are reported in table 2.

Table 2 Reactivation constants of **1** and **2** at 37°C for hAChE inhibited by various OP.

	k_r (min^{-1})	K_D (μM)	k_{r2} ($mM^{-1}min^{-1}$)[a]
VX			
2–PAM	0.1 ± 0.01	210 ± 60	0.51
HI-6	0.65 ± 0.03	70 ± 8	9.3
Obidoxime[b]	0.60 ± 0.05	54±12	11
1[b]	0.72 ± 0.07	31 ± 6	22
2	0.29 ± 0.02	21.3 ± 5.1	13.6
Sarin (NIMP)			
2–PAM	0.24 ± 0.02	210±30	1.18
HI-6	1.2 ± 0.2	90 ± 34	12.9
Obidoxime	0.17 ± 0.02	500 ± 95	0.34
1	0.33 ± 0.01	20 ± 3	16.5
2	0.14 ± 0.01	11.5 ± 3.1	12.2
Tabun			
2–PAM	0.15 ± 0.03	790 ± 190	0.2
HI-6	0.05 ± 0.005	200 ± 40	0.24
Obidoxime[b]	0.04 ± 0.006	250 ± 110	0.16
1[b]	0.021 ± 0.001	7.1 ± 1.5	3
2	0.12 ± 0.01	10.4 ± 2.6	11.5
Ethyl paraoxon			
2–PAM	0.054 ± 0.006	400 ± 80	0.14
HI-6	0.09±0.01	800 ± 140	0.1
Obidoxime	0.29 ± 0.02	550 ± 90	0.53

1[b]	0.111 ± 0.002	3.6 ± 0.2	31
2	0.11 ± 0.01	5.7 ± 1.7	19.2

[a] $k_{r2} = k_r/K_D$ [b] *from Kliachyna et al* [15].

Reactivator **2** outperformed 2-PAM, HI-6 and obidoxime. For the *VX*–hAChE conjugate, **2** is 27- more effective than 2–PAM and slightly better than HI–6 and obidoxime, respectively 1.5- and 1,2-fold. While it remained slightly less effective than reactivator **1**, reactivator **2** exhibited higher affinity (1.4-fold) for *VX*–AChE. For paraoxon–hAChE, **2** is 140- , 190- and 36-fold more effective than 2–PAM, HI–6 and obidoxime respectively. Towards the OP-hAChE conjugate obtained with the sarin surrogate, NIMP, **2** is 10- and 36-fold more effective than 2—PAM and obidoxime. It displayed effectiveness similar to that of HI-6, which is known to be quite efficient against sarin intoxication [5].

Quite remarkably, reactivator **2** exhibited the best reactivation potency for tabun poisoning. It is 4-fold more effective than **1**, and about 60-fold more effective than 2-PAM, HI-6 and obidoxime. The conjugates formed with tabun are known to be amongst the most difficult to reactivate, due to the weak electrophilicity of the phosphyl moiety and to the steric hindrance imposed on the phosphorus atom by the dimethylamino group in the hAChE-tabun adduct [21, 22].

Globally, this kinetic evaluation reveals that **2** is a very promising reactivator candidate with broad spectrum activity, and significantly less inhibitory potency than **1** in line with docking results. Based on the k_r and K_D constants reported in table 2, **2** attains theoretical clinically relevant concentrations for each OP evaluated by contrast to **1**, HI-6, obidoxime and especially 2-PAM (See Supplementary Information). Noteworthy, and similarly to what is measured for 2-PAM, HI-6 and obidoxime, the K_D of **2** for the different nerve agent conjugates is in the same order of magnitude as the IC_{50} for hAChE. This suggests that **2** should have a therapeutic window comparable to these oximes in regard to their side effects related to hAChE reversible inhibition.

X-ray structures of reactivator 2 in complex with *Tc*AChE and conjugates.

The structure of the *Tc*AChE-**2** complex is shown in Figure 5A. Each of the two monomers in the asymmetric unit, contains one molecule of **2** bound at the PAS, with aromatic stacking of Trp279, the tacrine moiety, and the pyridinaldoxime ring, as already observed for **1**. No copy of **2** can be seen at the bottom of the active site gorge, presumably due to the steric hindrance imposed by the chlorine substituent, as predicted. Despite the fact that PEG oligomers are not detected within the active site, the pyridinaldoxime does not point down the gorge as predicted by docking. The pocket formed at the gorge entrance by a symmetry-related protein copy probably dictates the orientation of the pyridinaldoxime moiety.

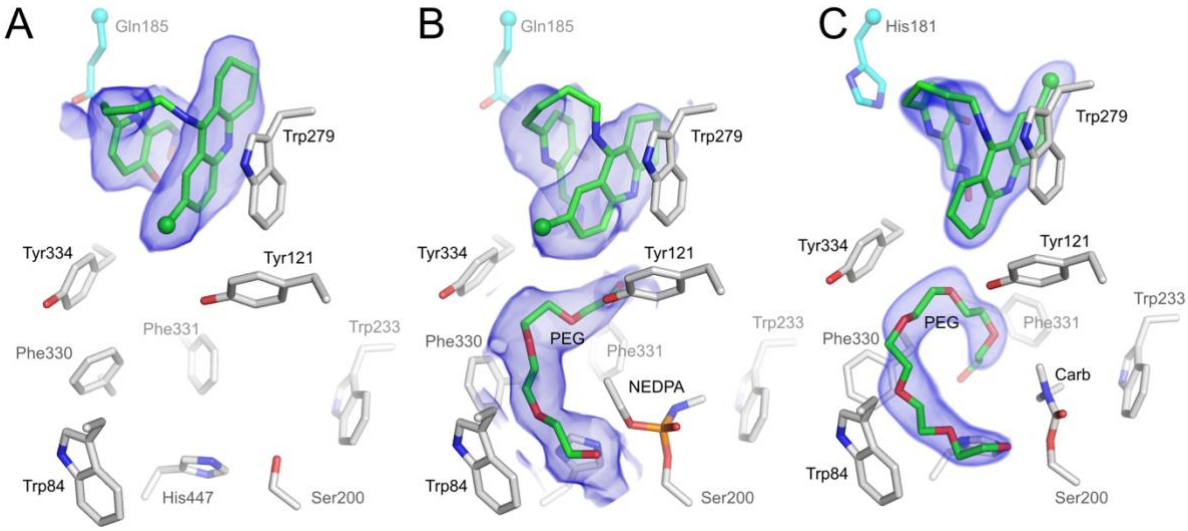

Figure 5 Crystal structures of unmodified *Tc*AChE and of its conjugates complexed with **2**. Volume represents feature enhanced maps (fem) contoured at 1 σ. A) *Tc*AChE-**2** complex (pdb 6g4n). One copy of **2** is seen at the PAS, while the active site is empty; B) NEDPA-*Tc*AChE-**2** complex (pdb 6g4p). A copy of **2** is seen, at the PAS, and a PEG oligomer from the crystallization conditions is seen alongside the phosphyl moiety; C) Carbamyl-*Tc*AChE-**2** (pdb 6fqn). A copy of **2** is clearly present at the PAS, while, again, a PEG oligomer is adjacent to the carbamyl moiety. The binding orientation of **2** at the PAS in the 3 panels is stabilized by Gln185 or His181 (cyan) of a symmetry mate specific of the crystal packing, thus partially artefactual.

We solved the structure of the NEDPA-*Tc*AChE-**2** ternary complex by successively soaking *Tc*AChE crystal first in NEDPA, and then in **2,** as had been done for **1** (Figure 5B). The

structure is very similar to that observed for the ternary complex of **1** with respect to the copy of reactivator binding at the PAS. However, no copy of **2** is present at the bottom of the gorge where the phosphyl adduct stabilizes a PEG molecule. The copy of **2** bound at the PAS is in the same orientation as in the non-phosphylated *Tc*AChE-**2** complex in both monomers A and B, thus confirming the affinity of **2** for the PAS of the inhibited enzyme.

The same holds true for the carbamyl-*Tc*AChE-**2** ternary complex (Figure 5C), which is virtually identical to carbamyl-*Tc*AChE-**1**, except that the orientation of the tacrine moiety can be unambiguously assigned due to the presence of the chlorine substituent.

Conclusion

We present the crystal structure of the complex of *Tc*AChE with the reactivator, **1**, which reveals a binding conformation within the active site that can account for its sub-millimolar inhibition of the enzyme. While AChE inhibition could protect against OP intoxication by transiently masking the active site from nerve agent [28], we developed a new molecule with the intention of limiting binding to the PAS, in a position which would permit favourable interaction of the aldoxime moiety with the covalently bound phosphyl group. To this end, **2**, bearing a chlorine at position 7 of the tacrine moiety was designed and tested by molecular docking before being synthesized. As predicted, the *in vitro* reactivation capability of **2** is comparable to that of **1**, but it is a 10-fold weaker inhibitor. Crystallographic data confirmed that it could bind only at the PAS of native *Tc*AChE, while preserving the same binding mode as **1** in the OP conjugates. The data presented demonstrate the value of rational design in refining the chemical structures of reactivator candidates, and support further investigation of **2** for *in vivo* evaluation studies.

Experimental Section

1. Chemicals

Chemicals including paraoxon were purchased from Sigma-Aldrich unless mentioned otherwise. The tabun analog, 4-nitrophenyl ethyl dimethylphosphoramidate (NEDPA), and the sarin surrogate 4-nitrophenyl isopropyl methylphosphonate (NIMP), were synthesized by Catherine Gomez (COBRA laboratory, UMR 6014, France) as described [26]. Stock solutions of 5 mM VX and tabun in isopropanol were obtained from DGA maîtrise NRBC (Vert le Petit, France). **1** was synthesized as previously published [15]. **2** was synthesized as described in the result section with details and analyses reported in the supplementary information file. Compound **1** and **2** were ≥ 95% pure as determined by HPLC and HRMS. They are water-soluble at concentrations up to 40 mM (higher concentration not tested). The rivastigmine analog was a gift from Ben Ross from the University of Queensland, synthesized by Satish Dighe (unpublished structure ; (S)-3-(1-(dimethylamino)ethyl)-5-hydroxy-phenyl ethyl(methyl)carbamate).

2. AChE preparations

Recombinant hAChE was produced and purified as previously described [22]. The G_2 form of *Tc*AChE was purified from electric organ tissue of *Torpedo californica* [29].

3. Inhibition measurements

Oximes were dissolved in MeOH to make 5 or 10 mM stock solution. Recombinant hAChE activity was measured spectrophotometrically at 25 °C, monitoring absorbance at 412 nm, in 1 mL Ellman's buffer (0.5 mM DTNB/0.1% BSA/5% MeOH/0.1 M phosphate, pH 7.4), in the presence of appropriate oxime concentrations. Measurements were performed at least in duplicate for each concentration tested. The oxime concentration producing 50% inhibition

was determined by non-linear fitting with ProFit (Quantumsoft) using the standard IC_{50} equation: %Activity = 100*IC_{50}/(IC_{50}+[Ox]).

4. Reactivation of hAChE inhibited by OPs

The inhibition of 120 µM hAChE was performed with a 5-fold excess of OP, in 0.1% BSA/20 mM Tris, pH 7.4, at 25 °C. After a 20-min incubation, the inhibited hAChE was desalted on a PD-10 column (GE Healthcare).

2-PAM and obidoxime chloride were from Sigma (Saint-Quentin Fallavier, France) and HI-6 from Pharmacie Centrale des Armées (Orléans, France). OP-inhibited hAChE was incubated at 37°C with at least four concentrations of the oxime in 0.1% BSA/0.1 M phosphate, pH 7.4. The final concentration of MeOH in the incubation mixture was <2%, and had no influence on the enzyme's activity. At time intervals of from 1-10 min, depending on the reactivation rate, 10-µL aliquots were transferred to cuvettes containing 1mM acetylthiocholine in 1 mL Ellman's buffer, for measurement of hAChE activity at 25 °C. The enzyme activity in the control, *viz.*, uninhibited enzyme + oxime, remained constant throughout the experiment. Oximolysis was undetectable.

The percentage of reactivated enzyme ($\%E_{react}$) was calculated as the ratio of the recovered enzyme activity and the activity in the control. The apparent reactivation rate, k_{obs}, for each oxime concentration, the dissociation constant, K_D, of inhibited enzyme-oxime complex (E-POx), and the reactivation rate constant, k_r, were calculated by non-linear fit with ProFit (Quantumsoft) using the standard oxime concentration-dependent reactivation equation derived from the following scheme:

$$\text{E-P} + \text{Ox} \underset{}{\overset{K_D}{\rightleftharpoons}} \text{E-POx} \xrightarrow{k_r} \text{E} + \text{POx}$$

$$\%E_{react} = 100 \,.\, (1\text{-}e^{k_{obs} \cdot t}) \qquad \text{and} \qquad k_{obs} = \frac{k_r[Ox]}{K_D + [Ox]}$$

The reactivator concentrations used for each set of experiments are given in the Supplementary Information.

5. Molecular docking

Flexible docking was performed using AutoDock Vina [30] as described before [15]. Briefly, the system was prepared in PyMOL (Schrödinger) using the plug-in developed by Daniel Seeliger (http://wwwuser.gwdg.de/~dseelig/adplugin.html). VX-hAChE was constructed from the apo form (pdb code 4ey4) by homology with the mAChE-VX structure (pdb code 2y2u), retaining in the active site all the usually conserved water molecules [31]. Residues in the gorge (Tyr72, Asp74, Trp86, Tyr124, Ser125, Trp286, Tyr337, Phe338, Tyr341; hAChE numbering) were selected as flexible, along with the ethyl group of VX. A 60 × 60 × 60 Å docking box was employed, centered near the bottom of the gorge, between Tyr124 and Trp86. Ligands were built and optimized from SMILEs string using phenix eLBOW [32]. The default parameter set of AutoDock Vina was used to generate 9 docking poses per molecule. The pose with the best energy score was selected as the most representative.

6. X-ray crystallography

Crystallization of *Tc*AChE utilized ~36% PEG200/150 mM MES, pH 5.6. The optimal concentration of PEG200 was determined for each batch of purified enzyme, and was in the range of 30-38%. Most crystals were of the orthorhombic form with only very few trigonal crystals among them. Trigonal crystals are usually of better quality and were used in priority when available. In both forms, a symmetric molecule faces the active site gorge entrances without occluding it, and surface residues Gln185 and His181 can eventually interact with PAS ligands.

To obtain tabun and NEDPA conjugates, the crystals were soaked in mother liquor containing 500 µM OP diluted in water from the stock solution. The affinities of the OPs for the enzyme, and their reactivities, are very high, so inhibition of the crystalline *Tc*AChE is limited mainly

by the diffusion of the OP into the solvent channels. The soaking of neutral reactivators **1** and **2** was performed at a concentration of 20 mM in dimethylsulfoxide (DMSO) at room temperature and subsequently diluting them in crystal mother liquor to a final concentration of 1mM. Soaking was times ranging from 2 min to 2 days were tested. The ternary complexes, *Tc*AChE-NEDPA-**1** and *Tc*AChE-NEDPA-**2,** were obtained by an initial soak of a few minutes with NEDPA, using the protocol described above, followed by a second one in a solution containing 1mM of reactivator and 500 µM OP to maintain the enzyme in a phosphylated state. Similarly, the ternary complexes carbamyl-*Tc*AChE- **1** and carbamyl-*Tc*AChE-**2** were obtained by an initial soak of a few minutes in mother liquor containing 500 µM of the rivastigmine analog, followed by a second soak in a solution containing 1mM of reactivator and 500 µM of the analog.

*Tc*AChE crystals can be cryo-cooled without further cryo-protection due to the presence of PEG200 in the crystallisation conditions. Diffraction data were collected at the ESRF, on MX beamlines ID14-4, ID23-1 and ID29 [33, 34], following the most appropriate strategy suggested by EDNA [35]. Datasets were either processed with XDS [36] or using the automatic processing output provided by the ESRF. Once the data had been scaled and truncated at a proper resolution, using the aimless-pointless pipeline in CCP4, native *Tc*AChE monomer (PDB entry 1ea5) was used as a starting model for molecular replacement by Phaser [37]. The resulting model was completed by iterative refinement in phenix.refine [38] and manual building with Coot [39]. Ligand models were built using phenix.eLBOW [32].

Supplementary information Detailed experimental procedures for the synthesis of **2** and analyses, reactivation kinetics for **1** and **2**, and clinically relevant concentrations of 2-PAM, HI-6, obidoxime, **1** and **2**. Molecular Formula Strings are available.

PDB ID Codes: Tabun-*Tc*AChE conjugate, 6g17; *Tc*AChE-**1**, 6g4n; NEDPA-*Tc*AChE-**1**, 6g4o; *Tc*AChE-**2**, 6g4m; NEDPA-*Tc*AChE-**2**, 6g4p. Authors will release the atomic coordinates upon article publication.

Corresponding Author Information. Département de Toxicologie et Risques Chimiques, Institut de Recherche Biomédicale des Armées, 1 place du Général Valérie André, BP73, 91223 Brétigny-sur-Orge, France ; Tel.: +33(0)178651877 ; email : florian.nachon@chemdef.fr

Author Contribution. [§]These authors contributed equally to this work. GS, EdlM and FN performed X-ray crystallography. GS and FN performed docking. JdS synthesized compound **1** and **2** under the supervision of RCDB and RB. JD and FN provided hAChE and performed the inhibition and reactivation kinetics. JLS and IS provided *Tc*AChE. All authors contributed to the writing and improvement of the manuscript.

Acknowledgement. GS and EdlM were supported by Direction Générale de l'Armement (DGA) through a grant from the ANR ASTRID program (ReCNSAChE). FN and JD were funded by the French Ministry of Armed Forces (DGA and SSA). JDS gratefully acknowledge the DGA, the Defence Science and Technology Laboratory (DSTL), UK, and the Centre National de la Recherche Scientifique (CNRS) for a research grant. The University of Strasbourg and the University of Southampton are also acknowledged for their support. We thank the ESRF staff for help during data collection.

Notes. The authors declare no competing financial interest.

Abbreviations used: AChE, acetylcholinesterase; TcAChE, *Torpedo californica* acetylcholinesterase; BBB, blood-brain barrier; CAS, catalytic aromatic site; PAS, peripheral aromatic site; PEG, polyethylene glycol

References

1. Silman, I.; Sussman, J. L. Acetylcholinesterase: 'classical' and 'non-classical' functions and pharmacology. *Curr. Opin. Pharmacol.* **2005,** 5, 293-302.
2. Mercey, G.; Verdelet, T.; Renou, J.; Kliachyna, M.; Baati, R.; Nachon, F.; Jean, L.; Renard, P. Y. Reactivators of acetylcholinesterase inhibited by organophosphorus nerve agents. *Acc. Chem. Res.* **2012,** 45, 756-766.
3. Sharma, R.; Gupta, B.; Singh, N.; Acharya, J. R.; Musilek, K.; Kuca, K.; Ghosh, K. K. Development and Structural Modifications of Cholinesterase Reactivators against Chemical Warfare Agents in Last Decade: A Review. *Mini Rev. Med. Chem.* **2015,** 15, 58-72.
4. Sakurada, K.; Matsubara, K.; Shimizu, K.; Shiono, H.; Seto, Y.; Tsuge, K.; Yoshino, M.; Sakai, I.; Mukoyama, H.; Takatori, T. Pralidoxime iodide (2-PAM) penetrates across the blood-brain barrier. *Neurochem. Res.* **2003,** 28, 1401-1407.
5. Worek, F.; Thiermann, H.; Szinicz, L.; Eyer, P. Kinetic analysis of interactions between human acetylcholinesterase, structurally different organophosphorus compounds and oximes. *Biochem. Pharmacol.* **2004,** 68, 2237-2248.
6. Lorke, D. E.; Kalasz, H.; Petroianu, G. A.; Tekes, K. Entry of oximes into the brain: a review. *Curr. Med. Chem.* **2008,** 15, 743-753.
7. Barckow, D.; Neuhaus, G.; Erdmann, W. D. Treatment of parathion (E 605) poisoning with the cholinesterase-reactivating substance obidoxime (Toxogonin). *Arch. Toxikol.* **1969,** 24, 133-146.
8. Clement, J. G.; Lockwood, P. A. HI-6, an oxime which is an effective antidote of soman poisoning: a structure-activity study. *Toxicol. Appl. Pharmacol.* **1982,** 64, 140-146.
9. Oldiges, H.; Schoene, K. Pyridinium and imidazolium salts as antidotes for soman and paraoxon poisoning in mice. *Arch. Toxikol.* **1970,** 26, 293-305.

10. Schoene, K.; Steinhanses, J.; Oldiges, H. Reactivation of soman inhibited acetylcholinesterase in vitro and protection against soman in vivo by bispyridinium-2-aldoximes. *Biochem. Pharmacol.* **1983,** 32, 1649-1651.
11. Sussman, J. L.; Harel, M.; Frolow, F.; Oefner, C.; Goldman, A.; Toker, L.; Silman, I. Atomic structure of acetylcholinesterase from Torpedo californica: a prototypic acetylcholine-binding protein. *Science* **1991,** 253, 872-879.
12. Kryger, G.; Harel, M.; Giles, K.; Toker, L.; Velan, B.; Lazar, A.; Kronman, C.; Barak, D.; Ariel, N.; Shafferman, A.; Silman, I.; Sussman, J. L. Structures of recombinant native and E202Q mutant human acetylcholinesterase complexed with the snake-venom toxin fasciculin-II. *Acta Crystallogr. D Biol. Crystallogr.* **2000,** 56, 1385-1394.
13. Ekstrom, F.; Hornberg, A.; Artursson, E.; Hammarstrom, L. G.; Schneider, G.; Pang, Y. P. Structure of HI-6*sarin-acetylcholinesterase determined by X-ray crystallography and molecular dynamics simulation: reactivator mechanism and design. *PLoS ONE* **2009,** 4, e5957.
14. Ekstrom, F.; Pang, Y. P.; Boman, M.; Artursson, E.; Akfur, C.; Borjegren, S. Crystal structures of acetylcholinesterase in complex with HI-6, Ortho-7 and obidoxime: structural basis for differences in the ability to reactivate tabun conjugates. *Biochem. Pharmacol.* **2006,** 72, 597-607.
15. Kliachyna, M.; Santoni, G.; Nussbaum, V.; Renou, J.; Sanson, B.; Colletier, J. P.; Arboleas, M.; Loiodice, M.; Weik, M.; Jean, L.; Renard, P. Y.; Nachon, F.; Baati, R. Design, synthesis and biological evaluation of novel tetrahydroacridine pyridine-aldoxime and -amidoxime hybrids as efficient uncharged reactivators of nerve agent-inhibited human acetylcholinesterase. *Eur. J. Med. Chem.* **2014,** 78, 455-467.
16. Korabecny, J.; Musilek, K.; Zemek, F.; Horova, A.; Holas, O.; Nepovimova, E.; Opletalova, V.; Hroudova, J.; Fisar, Z.; Jung, Y. S.; Kuca, K. Synthesis and in vitro

evaluation of 7-methoxy-N-(pent-4-enyl)-1,2,3,4-tetrahydroacridin-9-amine-new tacrine derivate with cholinergic properties. *Bioorg. Med. Chem. Lett.* **2011,** 21, 6563-6566.

17. Kuca, K.; Juna, D.; Musilek, K. Structural requirements of acetylcholinesterase reactivators. *Mini Rev. Med. Chem.* **2006,** 6, 269-277.
18. de Sousa, J.; Brown, R. C. D.; Baati, R. Buchwald-Hartwig Amination Approach for the Synthesis of Functionalized 1,2,3,4-Tetrahydroacridine Derivatives. *Eur. J. Org. Chem.* **2014,** 2014, 3468-3474.
19. Cross, R. M.; Maignan, J. R.; Mutka, T. S.; Luong, L.; Sargent, J.; Kyle, D. E.; Manetsch, R. Optimization of 1,2,3,4-tetrahydroacridin-9(10H)-ones as antimalarials utilizing structure-activity and structure-property relationships. *J. Med. Chem.* **2011,** 54, 4399-4426.
20. Renou, J.; Loiodice, M.; Arboleas, M.; Baati, R.; Jean, L.; Nachon, F.; Renard, P. Y. Tryptoline-3-hydroxypyridinaldoxime conjugates as efficient reactivators of phosphylated human acetyl and butyrylcholinesterases. *Chem. Commun. (Camb.)* **2014,** 50, 3947-3950.
21. Carletti, E.; Colletier, J. P.; Dupeux, F.; Trovaslet, M.; Masson, P.; Nachon, F. Structural evidence that human acetylcholinesterase inhibited by tabun ages through O-dealkylation. *J. Med. Chem.* **2010,** 53, 4002-4008.
22. Carletti, E.; Li, H.; Li, B.; Ekstrom, F.; Nicolet, Y.; Loiodice, M.; Gillon, E.; Froment, M. T.; Lockridge, O.; Schopfer, L. M.; Masson, P.; Nachon, F. Aging of cholinesterases phosphylated by tabun proceeds through O-dealkylation. *J. Am. Chem. Soc.* **2008,** 130, 16011-16020.
23. Millard, C. B.; Kryger, G.; Ordentlich, A.; Greenblatt, H. M.; Harel, M.; Raves, M. L.; Segall, Y.; Barak, D.; Shafferman, A.; Silman, I.; Sussman, J. L. Crystal structures of

aged phosphonylated acetylcholinesterase: nerve agent reaction products at the atomic level. *Biochemistry* **1999,** 38, 7032-7039.

24. Dym, O.; Song, W.; Felder, C.; Roth, E.; Shnyrov, V.; Ashani, Y.; Xu, Y.; Joosten, R. P.; Weiner, L.; Sussman, J. L.; Silman, I. The impact of crystallization conditions on structure-based drug design: A case study on the methylene blue/acetylcholinesterase complex. *Protein Sci.* **2016,** 25, 1096-1114.
25. Harel, M.; Schalk, I.; Ehret-Sabatier, L.; Bouet, F.; Goeldner, M.; Hirth, C.; Axelsen, P. H.; Silman, I.; Sussman, J. L. Quaternary ligand binding to aromatic residues in the active-site gorge of acetylcholinesterase. *Proc. Natl. Acad. Sci. U. S. A.* **1993,** 90, 9031-9035.
26. Meek, E. C.; Chambers, H. W.; Coban, A.; Funck, K. E.; Pringle, R. B.; Ross, M. K.; Chambers, J. E. Synthesis and in vitro and in vivo inhibition potencies of highly relevant nerve agent surrogates. *Toxicol. Sci.* **2012,** 126, 525-533.
27. Ellman, G. L.; Courtney, K. D.; Andres, V., Jr.; Feather-Stone, R. M. A new and rapid colorimetric determination of acetylcholinesterase activity. *Biochem. Pharmacol.* **1961,** 7, 88-95.
28. Lallement, G.; Baille, V.; Baubichon, D.; Carpentier, P.; Collombet, J. M.; Filliat, P.; Foquin, A.; Four, E.; Masqueliez, C.; Testylier, G.; Tonduli, L.; Dorandeu, F. Review of the value of huperzine as pretreatment of organophosphate poisoning. *Neurotoxicology* **2002,** 23, 1-5.
29. Sussman, J. L.; Harel, M.; Frolow, F.; Varon, L.; Toker, L.; Futerman, A. H.; Silman, I. Purification and crystallization of a dimeric form of acetylcholinesterase from Torpedo californica subsequent to solubilization with phosphatidylinositol-specific phospholipase C. *J. Mol. Biol.* **1988,** 203, 821-823.

30. Trott, O.; Olson, A. J. AutoDock Vina: improving the speed and accuracy of docking with a new scoring function, efficient optimization, and multithreading. *J. Comput. Chem.* **2010,** 31, 455-461.

31. Koellner, G.; Kryger, G.; Millard, C. B.; Silman, I.; Sussman, J. L.; Steiner, T. Active-site gorge and buried water molecules in crystal structures of acetylcholinesterase from Torpedo californica. *J. Mol. Biol.* **2000,** 296, 713-735.

32. Moriarty, N. W.; Grosse-Kunstleve, R. W.; Adams, P. D. electronic Ligand Builder and Optimization Workbench (eLBOW): a tool for ligand coordinate and restraint generation. *Acta Crystallogr. D Biol. Crystallogr.* **2009,** 65, 1074-1080.

33. de Sanctis, D.; Beteva, A.; Caserotto, H.; Dobias, F.; Gabadinho, J.; Giraud, T.; Gobbo, A.; Guijarro, M.; Lentini, M.; Lavault, B.; Mairs, T.; McSweeney, S.; Petitdemange, S.; Rey-Bakaikoa, V.; Surr, J.; Theveneau, P.; Leonard, G. A.; Mueller-Dieckmann, C. ID29: a high-intensity highly automated ESRF beamline for macromolecular crystallography experiments exploiting anomalous scattering. *J. Synchrotron Radiat.* **2012,** 19, 455-461.

34. Nurizzo, D.; Mairs, T.; Guijarro, M.; Rey, V.; Meyer, J.; Fajardo, P.; Chavanne, J.; Biasci, J. C.; McSweeney, S.; Mitchell, E. The ID23-1 structural biology beamline at the ESRF. *J. Synchrotron Radiat.* **2006,** 13, 227-238.

35. Incardona, M. F.; Bourenkov, G. P.; Levik, K.; Pieritz, R. A.; Popov, A. N.; Svensson, O. EDNA: a framework for plugin-based applications applied to X-ray experiment online data analysis. *J. Synchrotron Radiat.* **2009,** 16, 872-879.

36. Kabsch, W. XDS. *Acta Crystallogr. D Biol. Crystallogr.* **2010,** 66, 125-132.

37. McCoy, A. J.; Grosse-Kunstleve, R. W.; Adams, P. D.; Winn, M. D.; Storoni, L. C.; Read, R. J. Phaser crystallographic software. *J. Appl. Crystallogr.* **2007,** 40, 658-674.

38. Adams, P. D.; Afonine, P. V.; Bunkoczi, G.; Chen, V. B.; Davis, I. W.; Echols, N.; Headd, J. J.; Hung, L. W.; Kapral, G. J.; Grosse-Kunstleve, R. W.; McCoy, A. J.; Moriarty, N. W.; Oeffner, R.; Read, R. J.; Richardson, D. C.; Richardson, J. S.; Terwilliger, T. C.; Zwart, P. H. PHENIX: a comprehensive Python-based system for macromolecular structure solution. *Acta Crystallogr. D Biol. Crystallogr.* **2010,** 66, 213-221.

39. Emsley, P.; Lohkamp, B.; Scott, W. G.; Cowtan, K. Features and development of Coot. *Acta Crystallogr. D Biol. Crystallogr.* **2010,** 66, 486-501.

Table of Contents Graphic